Jurnal Penelitian dan Pengkajian Ilmu Pendidikan: e-Saintika
https://journal-center.litpam.com/index.php/e-Saintika/index

March 2025 Vol. 9, No. 1
e-ISSN: 2615-6881
pp. 1-12

Fabrication and Characterization of Supported Porous Au Nanoparticles

Ferry Anggoro Ardy Nugroho

Department of Physics, Faculty of Mathematics and Natural Sciences, Universitas Indonesia, Depok 16424, Indonesia

Corresponding Author e-mail: f.a.a.nugroho@sci.ui.ac.id

Received: November 2024; Revised: December 2024; Online First: December 2024; Published: March 2025

Abstract

Porous plasmonic nanoparticles offer unique advantages for sensing and catalysis due to their high surface-to-volume ratio and localized electromagnetic field enhancements at nanoscale pores, or "hotspots." However, current fabrication techniques, which are based on colloidal synthesis, face challenges in achieving precise control over particle size, shape, and porosity. Here, we present a robust nanofabrication method to produce supported arrays of porous Au nanoparticles with excellent dimensional and compositional control. By combining lithographically patterned AuAg alloy nanoparticles and selective dealloying via nitric acid, we achieve particle porosity without compromising particle morphology. Specifically, the method allows fabrication of supported porous nanoparticles with tunable dimension and porosity. Our approach demonstrates precise control of nanoparticle porosity by varying the initial Ag content in the alloy. Optical characterization reveals a blueshift in the extinction peak with increasing porosity, attributed to the reduced effective refractive index from intraparticle voids. Notably, a tunable shift of up to 100 nm in the plasmonic peak is observed, demonstrating the potential for fine-tuning optical properties. This study highlights the versatility of the proposed method in fabricating well-defined porous plasmonic nanoparticles and their ability to modulate optical properties through porosity control. These findings not only expand the toolkit for designing advanced plasmonic materials but also open pathways for applications in plasmon-mediated sensing, catalysis, and photonic devices.

Keywords: Nanoplasmonics, LSPR, Dealloying, Sensing, Catalysis, Nanotechnology

How to Cite: Nugroho, F. A. A. (2025). Fabrication and Characterization of Supported Porous Au Nanoparticles. *Jurnal Penelitian Dan Pengkajian Ilmu Pendidikan: E-Saintika*, *9*(1), 1–12. https://doi.org/10.36312/e-saintika.v9i1.2427

https://doi.org/10.36312/e-saintika.v9i1.2427

INTRODUCTION

Exploitation of localized surface plasmon resonance (LSPR) occurring in metal nanoparticles in the past two decades has opened the door to the realization of fascinating concepts and technologies, ranging from biological and chemical sensors (Nugroho et al., 2019; Tittl et al., 2018) to photonic devices (Dolia et al., 2024; Fusco et al., 2020; M. Zheng et al., 2023), optical metamaterials (N. Liu et al., 2009; Nugroho et al., 2022), and photocatalysts (Christopher et al., 2011; Yuan et al., 2022; Zhou et al., 2018, 2020). This is possible due to the fact that metal nanoparticles absorb and scatter light much more efficiently than their physical size would suggest at their resonance wavelength (Bohren, 1983). Furthermore, plasmonic nanoparticles act as deep sub-wavelength lenses by focusing light at their surface. Consequently, there exist

electromagnetic fields in the nanoparticles vicinity whose intensity is several times higher than the incoming light's. Driven by the exciting prospects of the potential applications, as well as by the need to understand these systems from a fundamental perspective, there exists a plethora of custom-designed nanoparticle shapes and arrangements (Becerril-Castro et al., 2022; J. Zheng et al., 2021). Furthermore, in the search for novel functionalities in plasmon-activated catalysis and plasmonic hydrogen sensing, new metals are being investigated beyond the traditional gold (Au) and silver (Ag), for instance palladium (Pd) (Langhammer et al., 2006; Nugroho et al., 2018) and aluminum (Al) (Knight et al., 2014; Swearer et al., 2016), and systems comprising several elements in the form of alloys (Nugroho et al., 2016a; Rahm et al., 2020; Wadell et al., 2015). The synergistic effects from the metal constituents enhance the functionality of the plasmonic alloys and provide an additional handle to tune their optical properties (Gong & Leite, 2016; Kadkhodazadeh et al., 2019).

A particularly interesting, yet rarely explored, feature with great potential for the creation of plasmonic nanostructures with novel functionalities is porosity (Koya et al., 2021). Inherent to this structure is the abundance of intramaterial nanogaps (*i.e.* the pores) which give rise to so-called "hotspots": regions where the local electromagnetic field is greatly enhanced with respect to the incoming field. The availability of accessible hotspots combined with large surface-to-volume ratios (SVR) makes porous metal nanoparticles uniquely suited for, *e.g.*, sensing and plasmon-mediated catalysis applications. Despite these prospects, however, relevant work in the literature has so far been limited to the use of porous plasmonic structures for surface-enhanced Raman scattering (SERS) (K. Liu et al., 2016; Q. Zhang et al., 2014; T. Zhang et al., 2018) and only using Ag or Au as the materials. One of the main contributing reasons for these limitations is that, so far, the porous nanoparticles have been mostly produced *via* colloidal synthesis, which introduces several limitations as described in details below.

At present, colloidal synthesis remains the main fabrication technique to produce porous nanoparticles (K. Liu et al., 2016; Q. Zhang et al., 2014). The use of colloidally synthesized nanoparticles for practical applications, in particular in plasmon-mediated sensing and chemical activation, inherits several challenges: (i) synthesis of *monodisperse* particles with controlled shape and size is typically difficult and ensemble experiments have to take into account the sample dispersity. (ii) it is challenging to synthesize monodisperse porous particles larger than ~30 nm (Rioux & Meunier, 2015), which is the size range most relevant for plasmonic applications. (iii) colloidal suspensions of nanoparticles are difficult to implement in solid-state devices due to problems with their integration in *arrays* on a surface with controllable density and uniformity in coverage. (iv) colloidal nanoparticles are typically stabilized by capping ligands (or surfactants) whose function is to promote the selected shape/facet production (Heuer-Jungemann et al., 2019). These ligands are tightly bound to the particle surface and can therefore strongly affect, or even hinder, their performance in sensing and catalysis. To partially alleviate problems related to particle integration to a surface and ligand contamination, an alternative method has been suggested (Wang & Schaaf, 2012). In this approach, nanoparticles are directly fabricated on a surface through solid-state dewetting of Au/Ag film. To induce pores formation, selective dealloying *via* wet chemical etching is utilized. This method offers easy integration of

the porous particle to a surface, however, with poor control of the size, arrangement and the pore dimension of the nanoparticles.

As a response, to fully exploit the potential offered by plasmonic porous nanoparticles, here we present a nanofabrication route to produce supported arrays of porous plasmonic nanoparticles with excellent dimension control. Our method relies on the combination of lithographically patterned nanoparticles and layer-by-layer annealing to produce supported random AuAg alloy nanoparticles with excellent dimension controlled. Here we chose Ag as a sacrificial metal because it is dissolvable in a number of acids. To induce porosity, we explore the use of nitric acid to selectively remove Ag, resulting in porous Au nanoparticles. Our findings reveal excellent dimension stability of the nanoparticles, with tunable porosity defined by the Ag composition. Such a control allows modification of the nanoparticle's optical properties, reaching a variation of 100 nm in the extinction spectrum. Finally, our findings demonstrate the advantages of combining lithographic patterning and selective dealloying, that is the direct integration of nanoparticles onto a surface, allowing for utilization in real devices.

METHOD

Sample Fabrication

To prepare the alloy samples, we follow the protocol reported in (Nugroho et al., 2016b). Here we reproduce the step-by-step process for the sake of completeness. Evaporation masks were nanofabricated using the hole-mask colloidal lithography (Fredriksson et al., 2007) on 1 × 1 cm^2 glass substrates (Borofloat) and on silicon wafer substrates. The steps taken were: (i) substrates were cleaned by ultrasonic agitation consecutively in acetone, isopropanol and de-ionized water. (ii) PMMA (MicroChem, 4 wt% diluted in anisole, Mw = 950,000) was spin-coated onto the substrates at 2,000 r.p.m. for 30 s followed by baking at 170 ^oC on a hotplate for 5 min. (iii) samples were subjected to a 5 s oxygen plasma (50 W, 250 mtorr, Oxford Plasmalab 80+) to enhance the hydrophilicity of the sample surface. (4) A polyelectrolyte solution (poly diallyldimethylammonium, Mw = 200,000–350,000, Sigma Aldrich, 0.2 wt% in Milli-Q water, Millipore) was pipetted on the surface of the samples and left for 30 s before rinsing in de-ionized water, depositing a monolayer positive charged on the polymer surface. (5) A suspension of negatively charged polystyrene beads (PS, 100 nm sulfate latex, Invitrogen, 0.2 wt% in Milli-Q water) was added to the surface. After 3 min incubation the suspension was rinsed away with dei-ionized water, and the samples were blown dry with nitrogen gas. (6) A 15-nm-thick Au film was evaporated using a E-Flex evaporator at a base pressure of 1×10^{-6} torr and evaporation rate of 1 Å s^{-1}. (7) The PS beads were removed by tape stripping, leaving a Au film with holes at the positions of the stripped PS beads. (8) The samples were subjected to 10 min oxygen plasma treatment (50 W, 250 mtorr, Oxford Plasmalab 80+) to etch through the PMMA layer exposed beneath the holes in the Au mask. (9) To fabricate the AuAg alloys, Au and Ag were deposited in sequence at the same deposition rate through the mask in tailored amounts. The thicknesses of each Au and Ag layer determined the final composition of the alloy particles. (10) The remaining PMMA layer was dissolved in acetone in a liftoff step, removing the mask from the sample and leaving only the nanodisk structures on the substrate. (11) Samples were soaked in isopropanol and blown dry with nitrogen. (12) The AuAg samples were annealed in a home-made flow

furnace under 4% H_2 in Ar (100 ml min−1) at 500 °C for 24 h. In this way, alloying of AuAg samples was achieved.

To selectively etch the Ag in the alloys, the samples were dipped in nitric acid (70%, Sigma Aldrich). After dipping for a prescribed time, the samples were relocated to Milli-Q water (Millipore) and left for 30 s, to remove the excess acid. Finally, the samples were blown dry with nitrogen gas. The simplified workflow for the proposed fabrication method is presented in Figure 1.

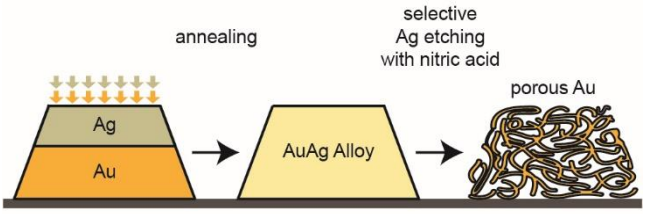

Figure 1. Conceptual illustration of porous Au nanoparticle fabrication strategy

First, a subsequent layer of consituent Au and Ag are deposited through a nanofabricated mask of a substrate. To induce complete alloying, the nanostructure is thermally annealed at a high temperature for a sufficient time. Last, the formed alloy is dipped in an etchant selective to only Ag, in this case a nitric acid, dealloying the nanosctructure back to comprise pure Au. The removal of Ag leaves Au nanostructure with pores, whose pore size is determined by the Ag content in the alloy.

Sample Characterization

Scanning electron microcopy (SEM) characterization, both for imaging and energy dispersive X-ray (EDX) analysis was conducted using FEI Verios 460 with 5 mm working distance.

ImageJ was used to determine the nanodisk diameter from the SEM images. To quantify the obtained diameters, a custom Matlab (R2023a) script was employed. For the histogram, we included $n > 500$ data. Furthermore, another Matlab script was also developed to obtaint the peak position (λ_{peak}) of the samples based on a Lorenztian fitting.

Data Analysis

ImageJ was used to determine the nanodisk diameter from the SEM images. To quantify the obtained diameters, a custom Matlab (R2023a) script was employed. For the histogram, we included $n > 500$ data. Furthermore, another Matlab script was also developed to obtaint the peak position (λ_{peak}) of the samples based on a Lorenztian fitting.

RESULTS AND DISCUSSION

Technological Barriers

To obtain supported Au nanoparticles with controlled porosity, we modified the widely used selective dealloying method (Vassileva et al., 2023). This approach begins with fully alloyed nanoparticles. Porosity is induced by using an etchant to selectively dissolve one alloy component, leaving the other intact but porous. Typically, acids serve as the selective etchant. In our work, we combined lithographically patterned nanoparticles with selective etching to produce arrays of supported porous nanoparticles (Figure 1). Specifically, we employed hole-mask colloidal lithography

(Fredriksson et al., 2007), layer-by-layer deposition, and annealing to fabricate nanoparticle arrays with tunable surface coverage, and precise particle dimensions and alloy compositions (Nugroho et al., 2016b). Hole-mask colloidal lithography also offers high scalability, as the process is driven by a self assembly process. Hence, this method offers significant advantages over approaches like dewetting, which provide limited control over particle size and composition. Notably, precise composition allows for high control over the pore dimensions in the resulting nanoparticles.

As shown in Figure 1, we used an AuAg alloy as a proof of concept for our study. We deposited alternating layers of Au and Ag *via* vapor deposition, followed by high-temperature annealing to produce fully alloyed AuAg nanoparticles (see Methods for details). Here we chose Ag as a sacrificial metal because it is dissolvable in many acids. To selectively remove Ag, we used nitric acid, which does not affect Au. This process left behind porous Au nanoparticles with minimal changes in their dimensions.

To demonstrate the viability of the proposed method, we fabricated the corresponding nanoparticles. First, we evaluated the efficacy of nitric acid in removing Ag and its impact on the composition and structure of the resulting particles (Figure 2). For this purpose, we prepared $Au_{80}Ag_{20}$ alloy nanodisks (composition confirmed by EDX analysis) with a nominal diameter of 100 nm and a height of 25 nm (Figure 2a,d). The Ag was selectively removed by dipping the samples in 70% nitric acid for 1 and 3 minutes. SEM images (Figure 2b,c) show that the etching process did not significantly alter the morphology, including particle diameter and surface coverage.

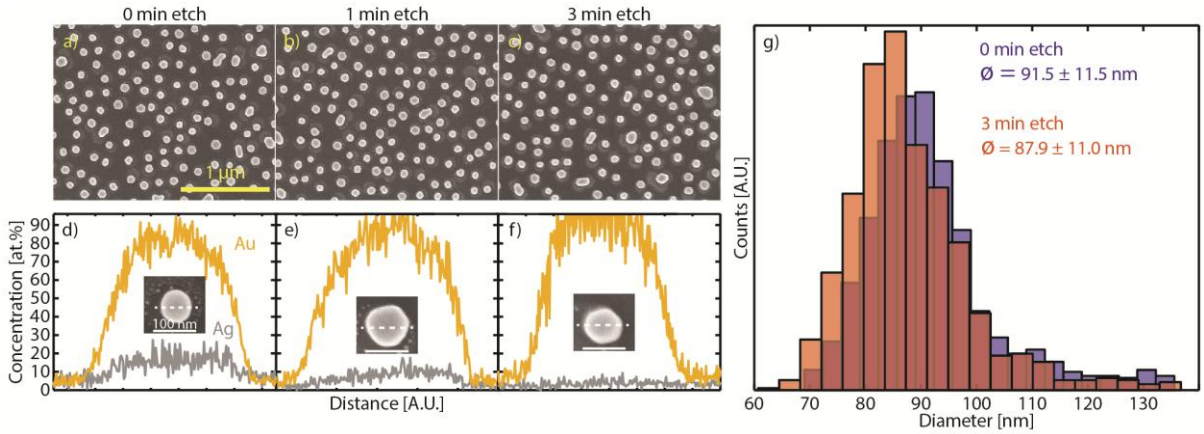

Figure 2. Compositional and morphological change of AuAg alloy nanodisks upon etching with nitric acid. SEM images of the $Au_{80}Ag_{20}$ nanodisks (Figure 2a) before and after etching with 0.5 M nitric acid for (b) 1 min and (c) 3 min. Upon etching, there is no apparent change on the shape and the coverage of the alloy nanoparticles. The corresponding composition linescan of a single nanodisk (d) before and after etching for (e) 1 min and (f) 3 min. Clearly, the amount of Ag gradually reduces with etching duration, until it completely diminishes after 3 min etching. (g) Diameter distribution histogram of the fabricated nanodisks before and after 3 min etching. The diameter of the nanodisk is practically unchanged, revealing that the structural integrity of the nanodisks is maintained despite Ag etching, which in turn indicates the formation of pores in the nanodisks.

In terms of composition, we observed a gradual reduction in Ag content with etching. After 1 minute, the particle composition shifted to approximately 90% at Au

(Figure 2e). Following 3 minutes, the Ag was entirely removed, resulting in pure Au nanodisks (Figure 2f). Notably, this compositional change was not accompanied by a significant morphological alteration. The removal of Ag was therefore associated with pore formation within the nanoparticles. To quantitatively confirm the minimal morphological changes, we constructed a histogram of nanodisk diameters before and after 3 minutes of etching (n > 500), as shown in Figure 2g. A minor shrinkage in particle diameter (< 4 nm) was observed.

At this point we have confirmed the complete removal of Ag and the structural integrity of the nanodisks. Together, these two findings heavily implies succesful pore formation in the nanoparticles. Ideally, direct morphological characterization such as transmission electron microscopy (TEM) is required to prove such a claim. However here TEM is not able to visualize the pores in our nanoparticles, as they seem to be small. Instead, we back up our claim of the pore formation with strong, indirect findings as we discuss in detail below.

Next, we proceeded to study the optical properties of our nanoparticles. We measured the extinction spectra of $Au_{80}Ag_{20}$ alloy nanodisks before and after 3 minutes of etching, using pure Au nanodisks of the same dimensions as a reference. As shown in Figure 3a, the alloy nanodisks exhibit a blueshift after etching due to the complete removal of Ag (Figure 3b). In contrast, the extinction spectra of the Au reference nanodisks remain constant, as expected, since Au does not react with the acid.

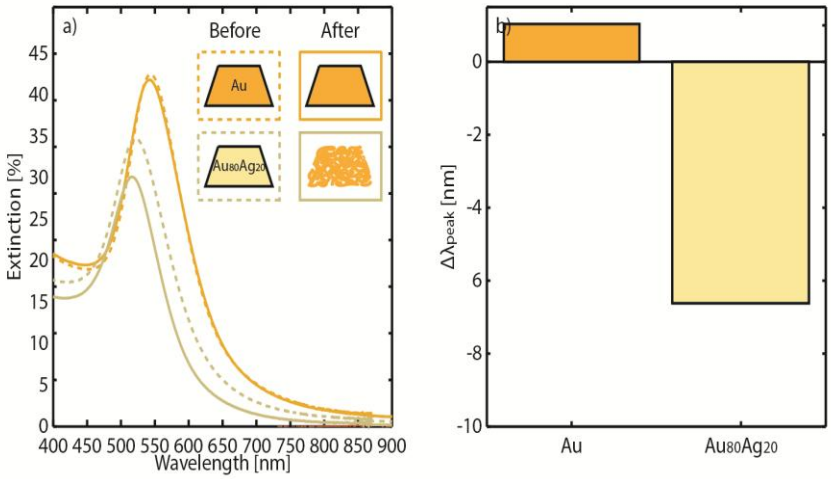

Figure 3. LSPR property change upon pore formation. (a) Extinction spectrum of pure Au and $Au_{80}Ag_{20}$ nanodisks before (dashed lines) and after (solid lines) 3 min ething (*i.e.* after pores are formed). Clearly, Au nanodisks exhibit constant extinction while $Au_{80}Ag_{20}$ does a blue shift, indicating the pore formation. Insets depict the morphological change of the nanodisks during etching. (b) Quantitative shift in the peak position, $\Delta\lambda_{peak}$, of the extinction spectrum of the nanodisks.

Since the overall dimensions of the alloy nanodisks remain unchanged after etching, we can conclude that the etched samples now have similar dimensions to the Au reference and consist solely of pure Au. Despite this similarity, Figure 3a clearly shows distinct optical properties between the two. This difference can be attributed to the presence of pores in the nanoparticles, further corroborating our argument of succesful pore formation above. Particularly, from a plasmonics perspective, these

pores introduce voids within the nanodisks' internal structure, reducing the overall refractive index of the system. Consequently, the plasmonic peak wavelength (λ_peak) of the porous nanoparticles shifts to a lower wavelength compared to solid nanoparticles, as observed here.

This finding not only confirms pore formation in the nanoparticles using our method but also highlights a potential strategy to tune the optical properties of nanoparticles by introducing porosity. As discussed above, the fabricated porous nanoparticles are readily integrated onto a support, allowing for utilization in real devices. This feature is markedly advantageous compared to, e.g., colloidally synthesized porous nanoparticles, where precise integration onto a support still constitutes a significant challenge (K. Liu et al., 2016; Q. Zhang et al., 2014).

In the final step of our study, we demonstrated how pore properties in nanoparticles influence their optical behavior. Specifically, we aimed to show that pore content affects the extinction spectrum of Au nanoparticles. Since our samples are supported nanoparticles, quantifying their pores (*e.g.*, pore size) using conventional methods like Brunauer-Emmet-Teller (BET) analysis is not feasible. Instead, we leveraged the relationship between pore content and the initial Ag composition during alloy fabrication. Higher initial Ag content leads to Au nanoparticles with greater porosity, and vice versa.

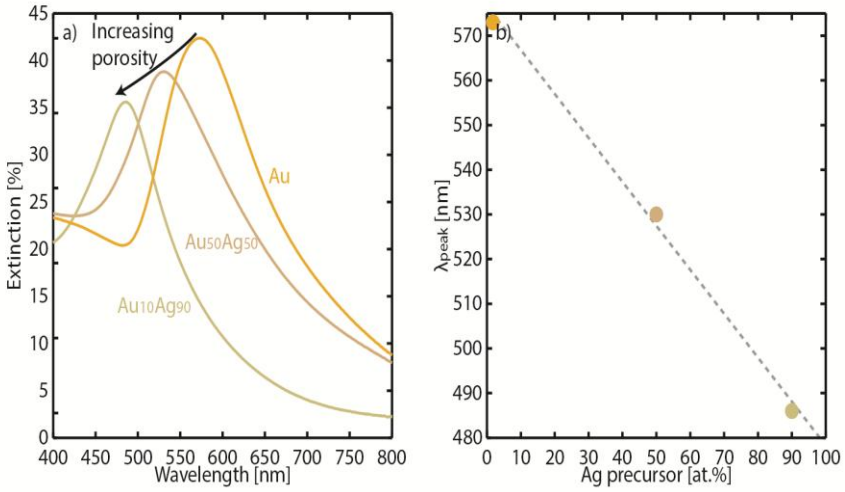

Figure 4. Impact of porosity on the LSPR property of porous Au nanodisks. (a) Extinction spectrum of Au with different porosity. Note that the labels mark the composition of the nanodisks before etching. After ethcing, the nanodisks are then comprises pure Au with different porosity defined by the prior composition of the Ag. Blue shifted λ_{peak} is observed for Au nanodisks with more pores (*i.e.* higher Ag composition). (b) The correlation between Ag composition and λ_{peak}. Dashed line is a guide to the eye.

To explore this, we fabricated three alloy nanoparticles of similar dimensions but different compositions: pure Au, $Au_{50}Ag_{50}$, and $Au_{10}Ag_{90}$. After etching, we measured and compared their extinction spectra. As shown in Figure 4a, the optical properties vary as expected, with the extinction peak exhibiting a blue shift as the initial Ag content—and consequently the pore content—increases. This supports our hypothesis that the voids in the nanoparticles reduce the overall refractive index of the system.

In Figure 4b, we quantify the differences in the plasmonic peak wavelength (λ_{peak}), noting that variations in porosity can induce shifts of up to 100 nm. This finding demonstrates that porosity provides an additional means to modify the plasmonic properties of materials, complementing traditional factors such as material composition, size, and shape.

CONCLUSION

This study establishes a robust nanofabrication approach to produce supported arrays of porous plasmonic nanoparticles with precise control over size, arrangement, and porosity. By combining lithographically patterned AuAg alloy nanoparticles with selective dealloying using nitric acid, we achieved porous Au nanoparticles with excellent dimensional stability and tunable porosity. Our findings demonstrate that the initial Ag composition directly influences the porosity, enabling systematic control over the nanoparticles' optical properties. Notably, we observed up to a 100 nm variation in the extinction spectrum, underscoring the significant impact of porosity on plasmonic behavior.

This work addresses the limitations of conventional colloidal and dewetting-based methods by offering superior control over nanoparticle dimensions and surface integration, critical for plasmonic applications. Moreover, the introduction of porosity as a design parameter provides a new avenue for tailoring the optical properties of plasmonic materials, expanding their potential applications in sensing (Alekseeva et al., 2019), catalysis (Pincella et al., 2014), and beyond. These advancements open pathways for further exploration of porous plasmonic nanostructures in practical devices and emerging technologies.

RECOMMENDATION

This work is limited to fabrication of porous Au nanoparticle through selective dealloying of AuAg. However, the fabrication concept is generic and can be extended to other systems. One compelling avenue is the fabrication of porous Pd nanoparticles using PdAl precursor alloys (which are miscible). By selectively etching Al from the alloy, it should be possible to create porous Pd structures with high surface area and abundant hotspots. These Pd nanoparticles hold significant promise for advanced applications, particularly in hydrogen sensing (Darmadi et al., 2020) and plasmon-mediated catalysis. Their intrinsic chemical affinity for hydrogen, combined with enhanced local field effects from their porous structure, makes them ideal candidates for highly sensitive and selective hydrogen detection. Similarly, the abundance of accessible hotspots in these structures could enhance catalytic reactions such as hydrogenation or dehydrogenation processes, making them valuable for catalytic applications.

Furthermore, a critical challenge in the development of such systems is the characterization and quantification of porosity. Traditional methods, such as BET surface area analysis, are incompatible with surface-supported nanoparticles. Therefore, future efforts should focus on developing or adapting techniques, such as advanced electron tomography or localized adsorption isotherms, to quantify pore size and distribution in supported systems. Addressing these challenges and exploring the proposed applications will unlock new functionalities and broaden the

scope of porous plasmonic nanoparticles in sensing, catalysis, and other emerging technologies.

Author Contributions

FAAN: Conceptualization, methodology, formal analysis, investigation, resources, writing, visualization, project administration, funding acquisition.

Funding

This research was funded by Hibah Publikasi Pascasarjana FMIPA UI 2024 No. PKS-046/UN2.F3.D/PPM.00.02/2024.

Conflict of interests

The author declares no conflict of interest, and the funder had no role in the design of the study, in the collection, analyses, or interpretation of data, in the writing of the manuscript, or in the decision to publish the results.

REFERENCES

Alekseeva, S., Nedrygailov, I. I., & Langhammer, C. (2019). Single Particle Plasmonics for Materials Science and Single Particle Catalysis. In *ACS Photonics* (Vol. 6, Issue 6, pp. 1319–1330). https://doi.org/10.1021/acsphotonics.9b00339

Becerril-Castro, I. B., Calderon, I., Pazos-Perez, N., Guerrini, L., Schulz, F., Feliu, N., Chakraborty, I., Giannini, V., Parak, W. J., & Alvarez-Puebla, R. A. (2022). Gold Nanostars: Synthesis, Optical and SERS Analytical Properties. *Analysis & Sensing*, *2*(3). https://doi.org/10.1002/anse.202200005

Bohren, C. F. (1983). How can a particle absorb more than the light incident on it? *American Journal of Physics*, *51*(4), 323. https://doi.org/10.1119/1.13262

Christopher, P., Xin, H., & Linic, S. (2011). Visible-light-enhanced catalytic oxidation reactions on plasmonic silver nanostructures. *Nature Chemistry*, *3*(6), 467–472. https://doi.org/10.1038/nchem.1032

Darmadi, I., Anggoro, F., Nugroho, A., & Langhammer, C. (2020). High-Performance Nanostructured Palladium-Based Hydrogen Sensors—Current Limitations and Strategies for Their Mitigation. *ACS Sensors*, *5*(11), 3306–3327. https://doi.org/10.1021/acssensors.0c02019

Dolia, V., Balch, H. B., Dagli, S., Abdollahramezani, S., Carr Delgado, H., Moradifar, P., Chang, K., Stiber, A., Safir, F., Lawrence, M., Hu, J., & Dionne, J. A. (2024). Very-large-scale-integrated high quality factor nanoantenna pixels. *Nature Nanotechnology*, *19*(9), 1290–1298. https://doi.org/10.1038/s41565-024-01697-z

Fredriksson, H., Alaverdyan, Y., Dmitriev, A., Langhammer, C., Sutherland, D. S., Zäch, M., & Kasemo, B. (2007). Hole-mask colloidal lithography. *Advanced Materials*, *19*(23), 4297–4302. https://doi.org/10.1002/adma.200700680

Fusco, Z., Rahmani, M., Tran-Phu, T., Ricci, C., Kiy, A., Kluth, P., Della Gaspera, E., Motta, N., Neshev, D., & Tricoli, A. (2020). Photonic Fractal Metamaterials: A Metal–Semiconductor Platform with Enhanced Volatile-Compound Sensing Performance. *Advanced Materials*, *32*(50), 2002471. https://doi.org/10.1002/adma.202002471

Gong, C., & Leite, M. S. (2016). Noble Metal Alloys for Plasmonics. *ACS Photonics*, *3*(4), 507–513. https://doi.org/10.1021/acsphotonics.5b00586

Heuer-Jungemann, A., Feliu, N., Bakaimi, I., Hamaly, M., Alkilany, A., Chakraborty, I., Masood, A., Casula, M. F., Kostopoulou, A., Oh, E., Susumu, K., Stewart, M. H., Medintz, I. L., Stratakis, E., Parak, W. J., & Kanaras, A. G. (2019). The Role of Ligands in the Chemical Synthesis and Applications of Inorganic Nanoparticles. *Chemical Reviews*, *119*(8), 4819–4880. https://doi.org/10.1021/acs.chemrev.8b00733

Kadkhodazadeh, S., Nugroho, F. A. A., Langhammer, C., Beleggia, M., & Wagner, J. B. (2019). Optical Property–Composition Correlation in Noble Metal Alloy Nanoparticles Studied with EELS. *ACS Photonics*, *6*(3), 779–786. https://doi.org/10.1021/acsphotonics.8b01791

Knight, M. W., King, N. S., Liu, L., Everitt, H. O., Nordlander, P., & Halas, N. J. (2014). Aluminum for Plasmonics. *ACS Nano*, *8*(1), 834–840. https://doi.org/10.1021/nn405495q

Koya, A. N., Zhu, X., Ohannesian, N., Yanik, A. A., Alabastri, A., Proietti Zaccaria, R., Krahne, R., Shih, W.-C., & Garoli, D. (2021). Nanoporous Metals: From Plasmonic Properties to Applications in Enhanced Spectroscopy and Photocatalysis. *ACS Nano*, *15*(4), 6038–6060. https://doi.org/10.1021/acsnano.0c10945

Langhammer, C., Yuan, Z., Zorić, I., & Kasemo, B. (2006). Plasmonic properties of supported Pt and Pd nanostructures. *Nano Letters*, *6*(4), 833–838. https://doi.org/10.1021/nl060219x

Liu, K., Bai, Y., Zhang, L., Yang, Z., Fan, Q., Zheng, H., Yin, Y., & Gao, C. (2016). Porous Au–Ag Nanospheres with High-Density and Highly Accessible Hotspots for SERS Analysis. *Nano Letters*, *16*(6), 3675–3681. https://doi.org/10.1021/acs.nanolett.6b00868

Liu, N., Liu, H., Zhu, S., & Giessen, H. (2009). Stereometamaterials. *Nature Photonics*, *3*(3), 157–162. https://doi.org/10.1038/nphoton.2009.4

Nugroho, F. A. A., Bai, P., Darmadi, I., Castellanos, G. W., Fritzsche, J., Langhammer, C., Gómez Rivas, J., & Baldi, A. (2022). Inverse designed plasmonic metasurface with parts per billion optical hydrogen detection. *Nature Communications*, *13*(1), 5737. https://doi.org/10.1038/s41467-022-33466-8

Nugroho, F. A. A., Darmadi, I., Cusinato, L., Susarrey-Arce, A., Schreuders, H., Bannenberg, L. J., da Silva Fanta, A. B., Kadkhodazadeh, S., Wagner, J. B., Antosiewicz, T. J., Hellman, A., Zhdanov, V. P., Dam, B., & Langhammer, C. (2019). Metal–polymer hybrid nanomaterials for plasmonic ultrafast hydrogen detection. *Nature Materials*, *18*, 489–495. https://doi.org/10.1038/s41563-019-0325-4

Nugroho, F. A. A., Darmadi, I., Zhdanov, V. P., & Langhammer, C. (2018). Universal Scaling and Design Rules of Hydrogen-Induced Optical Properties in Pd and Pd-Alloy Nanoparticles. *ACS Nano*, *12*(10), 9903–9912. https://doi.org/10.1021/acsnano.8b02835

Nugroho, F. A. A., Iandolo, B., Wagner, J. B., & Langhammer, C. (2016a). Bottom-Up Nanofabrication of Supported Noble Metal Alloy Nanoparticle Arrays for

Plasmonics. *ACS Nano*, *10*(2), 2871–2879. https://doi.org/10.1021/acsnano.5b08057

Nugroho, F. A. A., Iandolo, B., Wagner, J. B., & Langhammer, C. (2016b). Bottom-Up Nanofabrication of Supported Noble Metal Alloy Nanoparticle Arrays for Plasmonics. *ACS Nano*, *10*(2), 2871–2879. https://doi.org/10.1021/acsnano.5b08057

Pincella, F., Isozaki, K., & Miki, K. (2014). A visible light-driven plasmonic photocatalyst. *Light: Science & Applications*, *3*(1), e133. https://doi.org/10.1038/lsa.2014.14

Rahm, J. M., Tiburski, C., Rossi, T. P., Nugroho, F. A. A., Nilsson, S., Langhammer, C., & Erhart, P. (2020). A Library of Late Transition Metal Alloy Dielectric Functions for Nanophotonic Applications. *Advanced Functional Materials*, *30*(35), 2002122. https://doi.org/10.1002/adfm.202002122

Rioux, D., & Meunier, M. (2015). Seeded Growth Synthesis of Composition and Size-Controlled Gold–Silver Alloy Nanoparticles. *The Journal of Physical Chemistry C*, *119*(23), 13160–13168. https://doi.org/10.1021/acs.jpcc.5b02728

Swearer, D. F., Zhao, H., Zhou, L., Zhang, C., Robatjazi, H., Martirez, J. M. P., Krauter, C. M., Yazdi, S., McClain, M. J., Ringe, E., Carter, E. A., Nordlander, P., & Halas, N. J. (2016). Heterometallic antenna-reactor complexes for photocatalysis. *Proceedings of the National Academy of Sciences of the United States of America*, *113*(32), 8916–8920. https://doi.org/10.1073/pnas.1609769113

Tittl, A., Leitis, A., Liu, M., Yesilkoy, F., Choi, D. Y., Neshev, D. N., Kivshar, Y. S., & Altug, H. (2018). Imaging-based molecular barcoding with pixelated dielectric metasurfaces. *Science*, *360*(6393), 1105–1109. https://doi.org/10.1126/science.aas9768

Vassileva, Ev., Mihaylov, L., Lyubenova, L., Spassov, T., Scaglione, F., & Rizzi, P. (2023). Porous metallic structures by dealloying amorphous alloys. *Journal of Alloys and Compounds*, *969*, 172417. https://doi.org/10.1016/j.jallcom.2023.172417

Wadell, C., Nugroho, F. A. A., Lidström, E., Iandolo, B., Wagner, J. B., & Langhammer, C. (2015). Hysteresis-Free Nanoplasmonic Pd-Au Alloy Hydrogen Sensors. *Nano Letters*, *15*(5), 3563–3570. https://doi.org/10.1021/acs.nanolett.5b01053

Wang, D., & Schaaf, P. (2012). Nanoporous gold nanoparticles. *Journal of Materials Chemistry*, *22*(12), 5344. https://doi.org/10.1039/c2jm15727f

Yuan, Y., Zhou, L., Robatjazi, H., Bao, J. L., Zhou, J., Bayles, A., Yuan, L., Lou, M., Lou, M., Khatiwada, S., Carter, E. A., Nordlander, P., & Halas, N. J. (2022). Earth-abundant photocatalyst for H_2 generation from NH_3 with light-emitting diode illumination. *Science*, *378*(6622), 889–893. https://doi.org/10.1126/science.abn5636

Zhang, Q., Large, N., Nordlander, P., & Wang, H. (2014). Porous Au Nanoparticles with Tunable Plasmon Resonances and Intense Field Enhancements for Single-Particle SERS. *The Journal of Physical Chemistry Letters*, *5*(2), 370–374. https://doi.org/10.1021/jz402795x

Zhang, T., Sun, Y., Hang, L., Li, H., Liu, G., Zhang, X., Lyu, X., Cai, W., & Li, Y. (2018). Periodic Porous Alloyed Au–Ag Nanosphere Arrays and Their Highly Sensitive SERS Performance with Good Reproducibility and High Density of Hotspots. *ACS Applied Materials & Interfaces*, *10*(11), 9792–9801. https://doi.org/10.1021/acsami.7b17461

Zheng, J., Cheng, X., Zhang, H., Bai, X., Ai, R., Shao, L., & Wang, J. (2021). Gold Nanorods: The Most Versatile Plasmonic Nanoparticles. *Chemical Reviews*, *121*(21), 13342–13453. https://doi.org/10.1021/acs.chemrev.1c00422

Zheng, M., Shen, Y., Zou, Q., Huang, Y., Huang, K., She, X., & Jin, C. (2023). Moisture-Driven Switching of Plasmonic Bound States in the Continuum in the Visible Region. *Advanced Functional Materials*, *33*(3). https://doi.org/10.1002/adfm.202209368

Zhou, L., Martirez, J. M. P., Finzel, J., Zhang, C., Swearer, D. F., Tian, S., Robatjazi, H., Lou, M., Dong, L., Henderson, L., Christopher, P., Carter, E. A., Nordlander, P., & Halas, N. J. (2020). Light-driven methane dry reforming with single atomic site antenna-reactor plasmonic photocatalysts. *Nature Energy*, *5*(1), 61–70. https://doi.org/10.1038/s41560-019-0517-9

Zhou, L., Swearer, D. F., Zhang, C., Robatjazi, H., Zhao, H., Henderson, L., Dong, L., Christopher, P., Carter, E. A., Nordlander, P., & Halas, N. J. (2018). Quantifying hot carrier and thermal contributions in plasmonic photocatalysis. *Science (New York, N.Y.)*, *362*(6410), 69–72. https://doi.org/10.1126/science.aat6967